OBSERVATION OF SEA ICE CONDITIONS USING VISIBLE AND NEAR-INFRARED CHANNELS IN MOS-1/MESSR AND ADEOS/AVNIR

Kazuyuki Shirasaki[1], Hiroyuki Enomoto[1], Kazutaka Tateyama[1], Hideo Warashina[2] and Akihiko Watanabe[1]

[1]*Kitami Institute of Technology, 165, Koen-cho, Kitami 090-8507*
[2]*Sendai College of Technology, 1, Kitahara, Kamiayashi, Aoba-ku, Sendai 989-3124*

Abstract: This study investigated the surface condition of sea ice using visible and near-infrared radiometers (MOS-1/MESSR, ADEOS/AVNIR). When sea ice is newly formed in the early stage of the freezing season, it has low albedo. In particular, when the size of each ice floe is smaller than the spatial resolution of the radiometer, such sea ice area will be observed as an area of low albedo. The newly formed sea ice is difficult to distinguish from a pack ice area with low concentration in the early freezing season. Observation of thin sea ice using brightness temperature is difficult since thin sea ice has a similar brightness temperature to open water. Through the satellite observation of visible and near-infrared radiometers, this study focused on distinguishing ice types, focusing especially on newly formed ice. To observe the spectral characteristics of such ice type, this study carried out *in situ* observations. In the case of a wet surface or ice particles suspended in the water, although the albedo in the visible region is high, the albedo in the near-infrared region is low. This results are useful to discriminate between low concentration ice cover and thin or newly formed ice.

1. Introduction

Observations of sea ice have been carried out often, using passive microwave remote sensing. Visible images with fine spatial resolution are used to determine the surface condition. Satellite observations of sea ice focused mainly on their distribution and concentration. This study tried to develop a new method for estimating the surface condition of sea ice using near-infrared and visible radiometer data.

As a characteristic feature of sea ice in the early freezing season, frazil ice can be observed (Weeks and Ackley, 1986). Sea ice has a high production rate in autumn. Formation of frazil ice in the autumn contributes greatly to heat exchange between the ocean and atmosphere (Ushio and Wakatsuchi, 1993). Observation of frazil ice using satellite data is important for the early detection of ice formation (Enomoto *et al.*, 1996). A new method for observing the early stage of sea ice formation could contribute greatly to research on ice growth. This study used MESSR (Multispectral Electronic Self-Scanning Radiometer) and VTIR (Visible and Thermal Infrared Radiometer) aboard the MOS-1b (Marine Observation Satellite-1b), and also AVNIR (Advance Visible and Near-Infrared Radiometer) on the ADEOS (Advanced Earth Observing Satellite). MESSR and AVNIR have fine spatial resolutions, and they can

measure some parameters related to ice conditions, such as concentration, form of floating ice and stage of development.

This study also included a field experiment using portable visible and near-infrared spectrometers to compare spectral information on various ice types and satellite data.

2. Data

This study used satellite data on selected sea ice areas in the Antarctic in 1993 and in the Sea of Okhotsk in 1997 (Fig. 1a and 1b). Satellite images are available which show thin ice in the early freezing season. Table 1 summarizes the satellite data of MESSR and VTIR on MOS-1, and of AVNIR on ADEOS, which are used in this study. MESSR has a spatial resolution of 50 m. VTIR has spatial resolutions of 0.9 km in the visible and 2.7 km in the infrared bands. AVNIR has a spatial resolution of 16 m in multispectral mode. Observation wavelengths of each radiometer are sum-
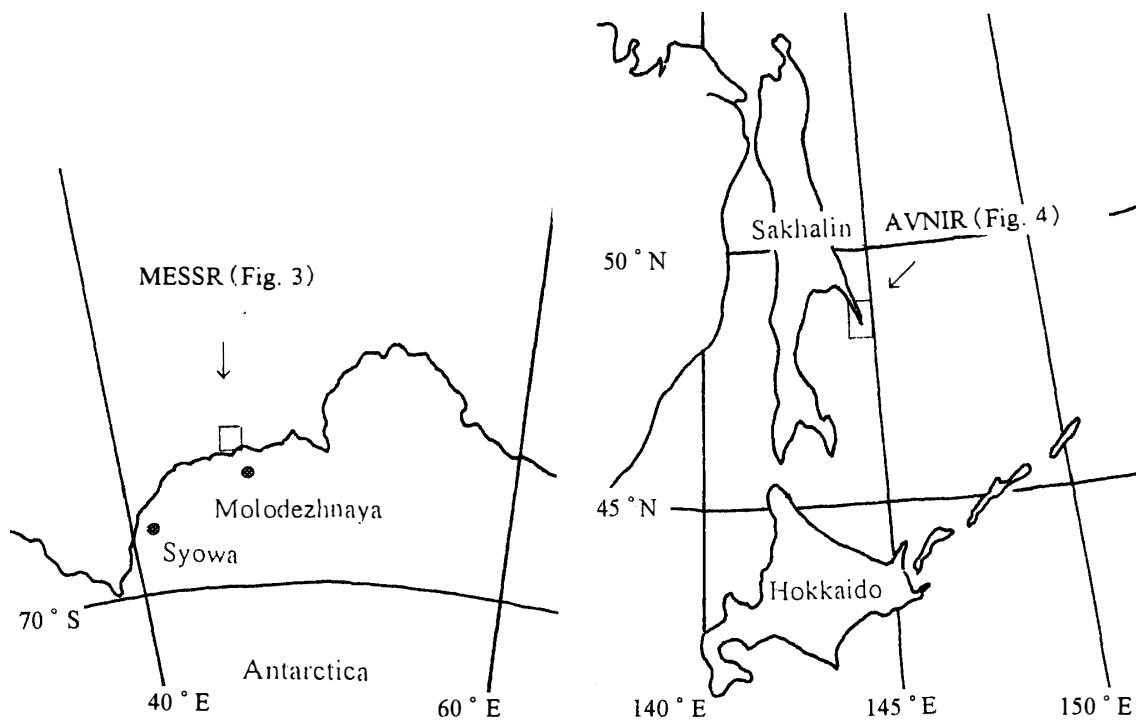

Fig. 1a. A area observed by MOS-1b VTIR in the Antarctic. The area observed by MESSR is indicated by a square.

Fig. 1b. Area observed by ADEOS AVNIR in the Sea of Okhotsk.

Table 1. Satellite data used in this study.

VTIR	MESSR	AVNIR
1993/04/07	1993/04/07	1997/02/07
1993/12/30		

Table 2.   Observation wavelength of each radiometer.
(μm)

	VTIR	MESSR	AVNIR
ch1	0.5–0.7	0.51–0.59	0.42–0.50
ch2	6.0–7.0	0.61–0.69	0.50–0.60
ch3	10.5–11.5	0.72–0.80	0.60–0.69
ch4	11.5–12.5	0.80–1.1	0.76–0.89

marized in Table 2.

In order to discuss results of satellite observation, spectral albedos for some typical conditions were collected using a portable field spectrometer (Ocean Optics Inc., PS-1000) in the spectral range of 0.4–1.1 μm.

3. Observation Using Visible and Thermal-infrared Channels

This study investigated seasonal differences in spectral characteristics of sea ice and compared them with those of cloud and open water in freezing and melting periods, using VTIR data around Antarctica. Some typical areas were selected in the VTIR images and their CCT (Computer Compatible Tape) digital counts were obtained. The CCT digital counts can be converted to albedo and brightness temperatures by the following formulas;

ch1 $A \ [\%] = I_v \ / \ 2,$ (1)
ch2, ch3, ch4 $T \ [\mathrm{K}] = I_\lambda \ / \ 2 + 233.16,$ (2)

where A is albedo [%], T is brightness temperature [K] and I_λ is CCT digital count (NASDA EOC, 1987). Sampled open water, cloud, and ice data are shown in Fig. 2. Data are shown as mean values over about 100 pixels (5 pixels for rock) for each channel.

Figure 2 shows that the albedos of all surface types were less than 10% in the freezing period. Cloud and sea ice have similar patterns but there are slight differences. Albedo of cloud is high compared to that of sea ice, but the brightness temperature of cloud is low compared to that of sea ice. The temperature of the sea ice area varies in a similar range to that of open water temperature in the melting period. When this temperature is close to the freezing point (271 K), it is difficult to distinguish open water and sea ice from the thermal data during the melting period.

It is easy to distinguish open water from sea ice by brightness temperature during the winter; however, distinguishing open water from sea ice by brightness temperature becomes difficult during the melting period and the freezing period. Ice concentration is calculated often from thermal-infrared data, but this becomes difficult in the melting and freezing seasons. Thin ice and grease ice in those seasons show similar values with the brightness temperature of open water. If thin ice or grease ice covers the observation area, it can be recognized as sea ice area of low concentration, using thermal-infrared data. In order to distinguish between a thin sea ice area and a low concentration sea ice area, this study investigated surface conditions of sea ice
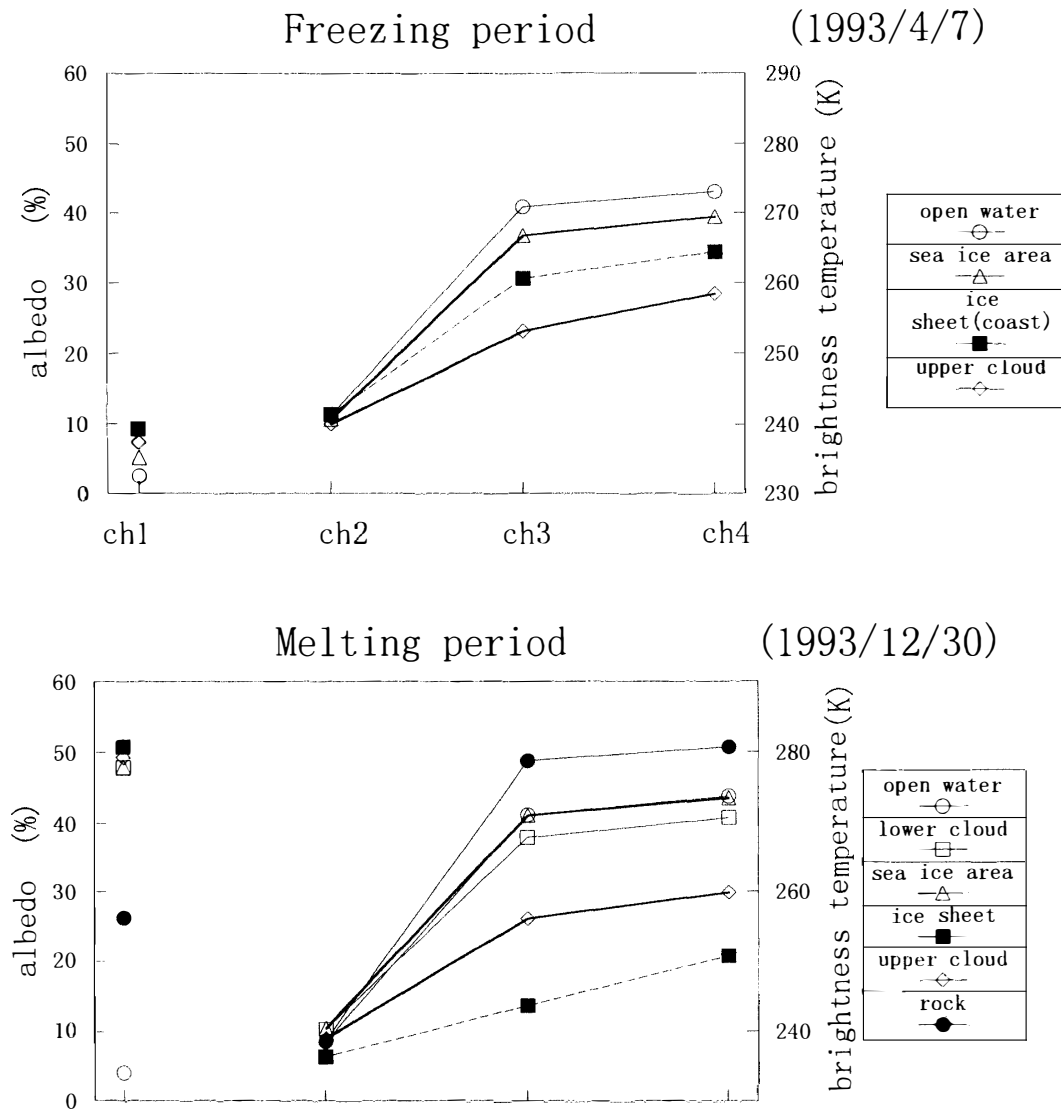
Fig. 2. *Sampled data of each parameter in the freezing and melting periods observed by VTIR. Mean values for each parameter are indicated. ch1: albedo. ch2, ch3, ch4: brightness temperature.*

using visible and near-infrared data, as reported in the next chapter.

4. Observation by Visible and Near-Infrared Channels

4.1. Satellite images of thin/new ice area

The large scale distribution of sea ice can be observed by VTIR. However, for observation of ice type and detailed distribution of sea ice, sensors with high spatial resolution such as MESSR or AVNIR are useful. Sea ice around the Antarctic during the freezing season in 1993 was analyzed using MESSR, which has fine spatial resolution (50 m). Figure 3 shows the sea ice area near Molodezhnaya Station, east of
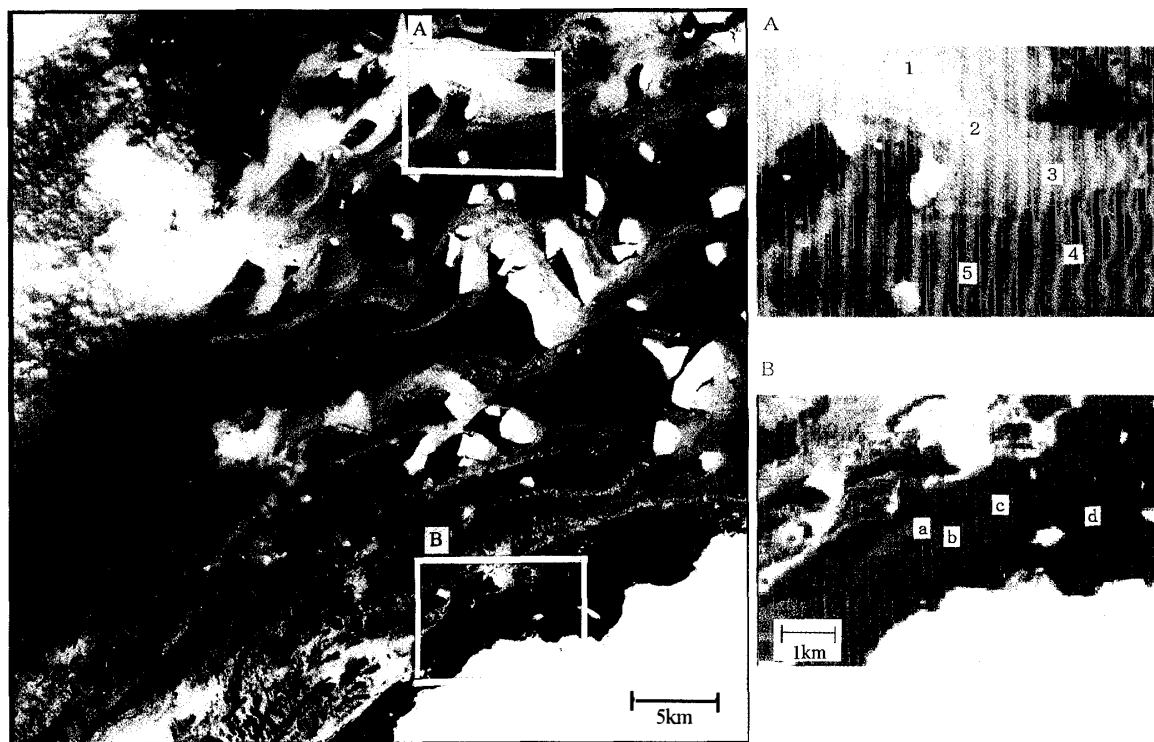
Fig. 3.   Sea ice area near Molodezhnaya Station, Antarctica, observed by MOS-1/MESSR, on 7 April
         1993. The sampled areas are shown with Nos. 1–5 and a–d. (color composition, R: ch1 G: ch2
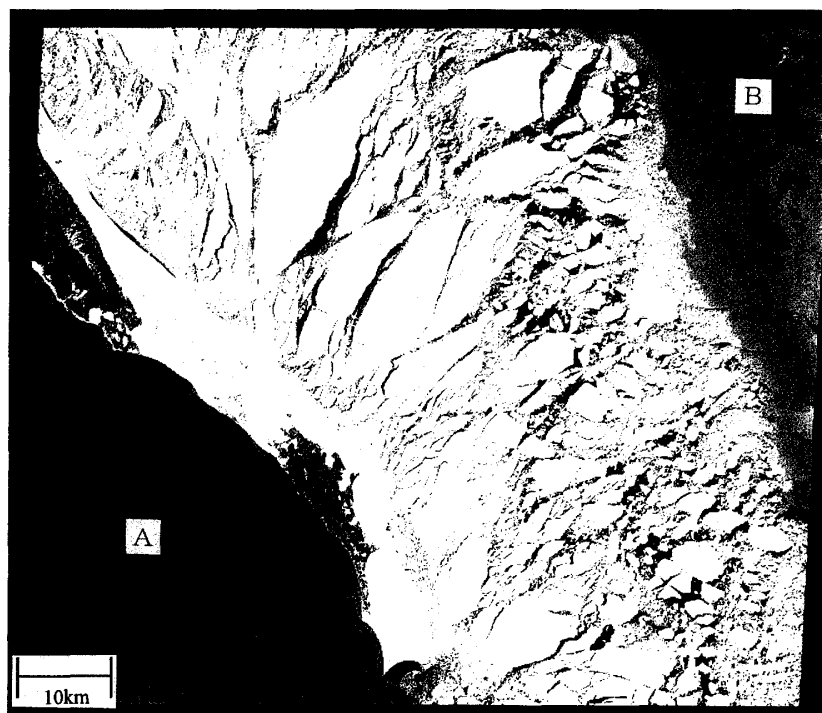   B: ch4).

Fig. 4.   AVNIR image of sea ice in the Sea of Okhotsk, near Sakhalin, on 7 February 1997. Point B is
         a new ice area. Point A is a nilas area. Top: north. (color composition, R: ch4 G: ch3 B: ch2).

Syowa Station, on 7 April 1993. Sampled areas are shown as areas No. 1–5 and a–d in Fig. 3. Digital counts on each channel were taken from various sea ice areas (1–5, a–d) in the satellite images.

The sea ice areas in Nos. 1–5 are located far from the coast. They are shown as bright areas in Fig. 3. Positions a–d are located near the coast. These regions (a–d) are shown with the dark region in Fig. 3. These areas are considered to be covered by sea ice because the albedos of these regions are slightly higher than those of open water. Sea ice was often blown away from the coast due to offshore wind; then the coastal open water expanded. New sea ice can be expected to form in such areas.

Sea ice data in the Sea of Okhotsk can also be analyzed using visible and near-infrared radiometers. New ice formation in the coastal open water can be observed frequently in the Sea of Okhotsk. Much of the Sea of Okhotsk, especially in the north and west areas and along Sakhalin, is covered by thin ice (ENOMOTO, 1996). The more advanced sensor, AVNIR, was utilized for these observations. An AVNIR image near Sakhalin is shown in Fig. 4. A nilas area can be seen west of the peninsula, and ice floes in the eastern region (Fig. 4). The thin ice area can be enhanced using near-infrared channels, as shown in Figs. 3 and 4.

4.2. Near-infrared/visible ratio

This study considers the ratio of near-infrared to visible (hereafter called the N_{ir}/V_{is} ratio) sea ice images. The N_{ir}/V_{is} ratio was obtained from CCT count data and plotted
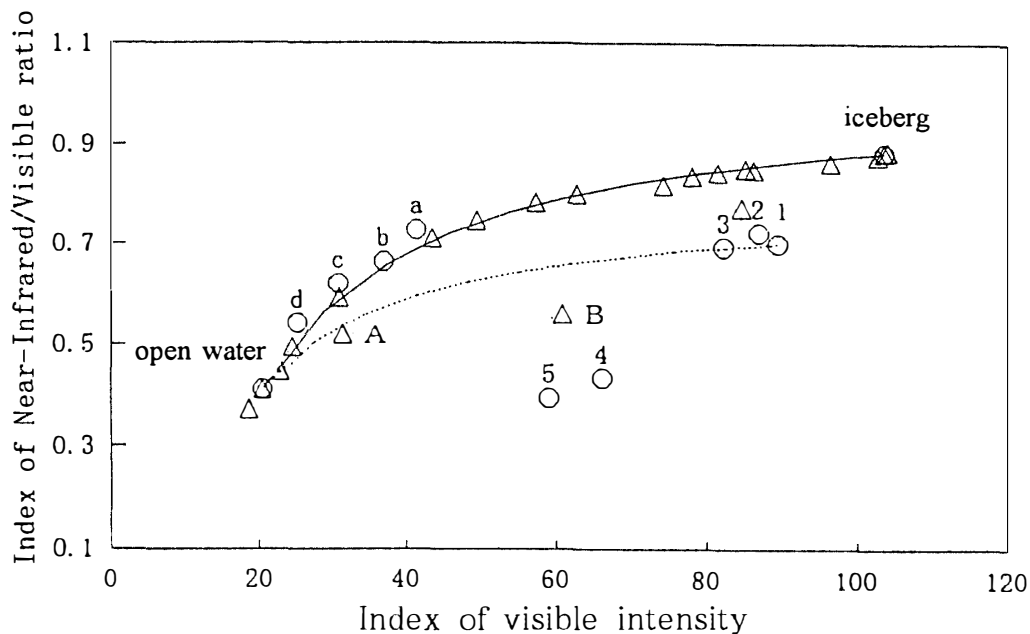

Fig. 5. *Relationship between intensity of visible range and the near-infrared/visible ratio. $\triangle$: AVNIR, $\bigcirc$: MESSR.*

Areas A and B correspond to areas in Fig. 4. Areas 1–5 and a–d correspond to areas in Fig. 3. The solid (dot) curve is calculated by changing areal ratio of open water area with iceberg (sea ice) area by adopting the spectral range of MESSR. Near-infrared: MESSR (ch4), AVNIR (ch4). Visible: MESSR (ch1), AVNIR (ch2).

as the ordinate (Fig. 5). Ranges of data distributions of MESSR and AVNIR were adjusted, simply by taking same and points for both data. Therefore both coordinates indicate relative values. This study uses this value as "index". Figure 5 shows the results after these adjustments.

If an area is covered by thick ice, the visible range index reflects the area of ice coverage. However, when the sea ice area is covered by thin ice which has lower albedo, the decrease of albedo does not reflect a decrease of ice coverage but rather a difference of ice type. This study uses the N_{ir}/V_{is} ratio to indicate this difference. The circle symbols in Fig. 5 are sampled MESSR data and the numbers correspond to those in Fig. 3. Triangles are sampled AVNIR data. The solid curve was drawn by changing areal ratio of open water and iceberg for each spectral bands.

$$C_{mix,i} = C_{ice,i} \times I_c + C_{water,i} \times (1 - I_c), \tag{3}$$

where C_{mix} : CCT counts of area covered by ice-water mixture,
  C_{ice} : CCT 100% ice concentration count data,
  C_{water} : CCT open water count data,
  I_c : ice concentration,
  i : channel.

The N_{ir}/V_{is} ratio was calculated by dividing the near-infrared channel C_{mix} by the visible channel C_{mix}. Near-infrared channels used are ch4 for MESSR and ch4 for AVNIR. Visible channels used are ch1 for MESSR and ch2 for AVNIR. The dotted line is calculated by changing the areal ratio of open water area to the brightest sea ice, not icebergs. An iceberg has a large near-infrared/visible ratio. Most data are expected to lie on either the solid or dotted line.

Sampled AVNIR and MESSR data for various ice concentrations are distributed along the line in Fig. 5. AVNIR data (triangles) along the line in Fig. 5 were obtained in the ice floe region, by selecting areas of various concentrations, in the area east of the peninsula in Fig. 4. Intensities of the channel varied due to ice concentration. However, sea ice in areas No. 4 and 5 have lower N_{ir}/V_{is} ratios. These lower values should be not only due to ice concentration but also due to surface conditions. Values for each sea ice area were averaged over several pixels. Using the relationships in Fig. 5, sea-ice concentration and difference of ice type can be analyzed. If the observed data are distributed along the solid line in Fig. 5, the sea ice area is considered to be covered with ice floes. On the other hand, when the observed data are scattered below the line, those ice types are considered to be different ice types. Points No. 4 and 5 are examples of this. Such a data point for AVNIR (B in Fig. 5) was obtained in the upper-right corner of Fig. 4 where new ice covered the ocean. Although points a–d in Fig. 3 might be an area of new ice formation, MESSR could not detect differences among the data points (a–d) as shown in Fig. 5. These data points are distributed above the solid line in Fig. 5. This higher value is considered to be due to the low gain of MESSR ch1 (V_{is}). AVNIR could detect the nilas (lower-left corner of Fig. 4) as indicated by data point A in Fig. 5.

4.3. Comparison with experiments

In order to investigate ice conditions with low near-infrared albedo which are seen

in Fig. 5, experimental observations were performed using a visible and near-infrared spectrometer (Ocean Optics Inc., PS1000, 0.4–1.1 μm). Albedo was calculated by dividing the observed spectral intensity from the material by that from a reference white board (diffuse reflectance target). Experiments were carried out by adding snow to water in a container. The spectral radiance was measured from the mixture of water and snow. This experiment was carried out *in situ* by using a halogen lamp as illumination. At the beginning of observation, snow was separated into floating particles which were suspended in the water. By adding more snow, snow particles were piled up and appeared near the water surface. Eventually, the snow protruded above the water level. The upper surface of this snow was not covered by water.

Field observations were also carried out in Lake of Saroma in Hokkaido, Japan. Figure 6 shows the results of observations. This figure shows the relationship between the N_{ir}/V_{is} ratio and albedo in the visible range. Visible and near-infrared observations were done in almost the same range of MESSR ch1 and ch4. The coverage of dry snow is 100% at the right end of this line and it is 0% (*e.g.*; water) at the left end. The solid line in Fig. 6 is calculated by changing the areal ratio of dry snow area and water area, with calculation done similarly to that for the lines in Fig. 5. The dots in Fig. 6 are observed values for wet snow. In the case of a wet surface or ice particles suspended in water, albedo in the visible region was high but albedo in the near-infrared region was low.

Ice particles suspended in water are visible due to the scattering of visible light; however, in the near-infrared range, such ice particles could not be detected because
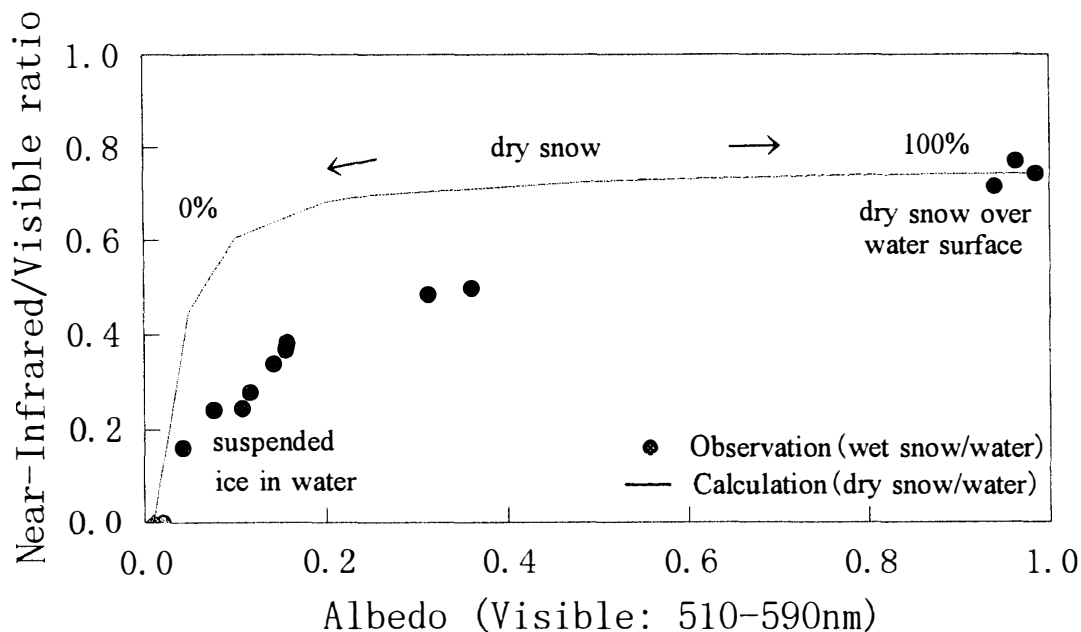

Fig. 6. *Results of experiment for mixture of snow and water. Relationships between albedo in the visible range versus the near-infrared/visible ratio. Observation data for wet snow and water were scattered below the line calculated for dry snow and water.*

the ice surface was still covered by water which has little reflectance in the near-infrared range. Therefore, the N_{ir}/V_{is} ratio is lower in this case and they are distributed out of line. With increasing wetness of snow, the N_{ir}/V_{is} ratio is expected to decrease. Results of satellite observation (Fig. 5) correspond to this type of ice.

ROGER et al. (1995) offered results of field observation of sea ice in the Antarctic at the onset of melt conditions. They observed that visible and near-infrared sea-ice albedo decreased due to water content within the snow and ice volumes and decrease of infrared albedo was remarkable compared to visible albedo. Although visible albedo was found to be sensitive to both ice surface and water layer, larger changes appeared in the near-infrared albedo due to the water layer over the ice. These results were similar to the results of the present study, since a wet surface affects the near infrared range considerably but the visible range less.

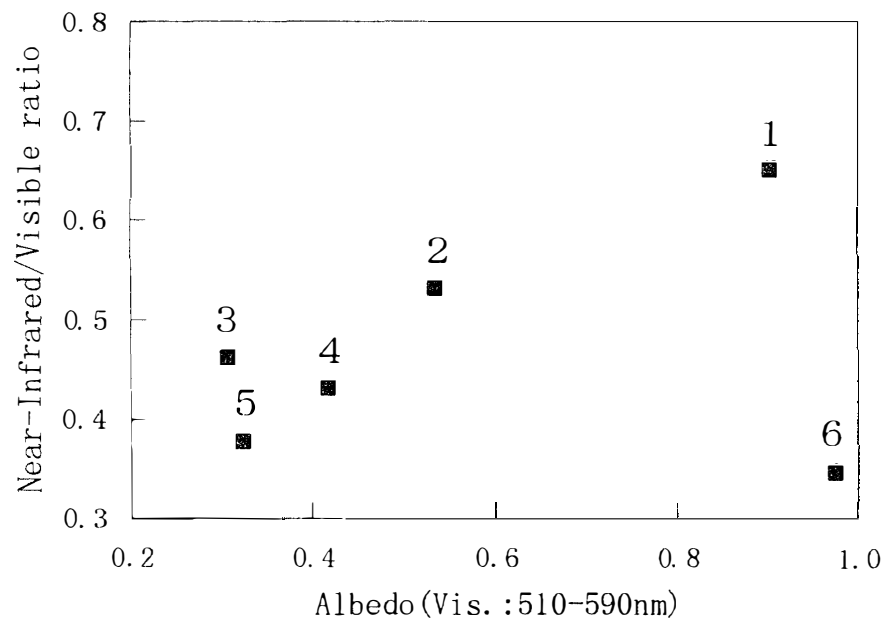Figure 7 shows results of field observations using PS-1000 (condition: fine weath-

Fig. 7.   Results of field observations at Lake Saroma, Hokkaido (January 20, 1997). Relationship between near-infrared/visible ratio and albedo in the visible range. Numbers in this figure correspond to those in Table 3.

Table 3.   Surface conditions of sea ice (January 1997).

Surface condition	Brightness	Roughness	Wetness
1. Snow covered	◯	✕	✕
2. Wet bare ice	✕	✕	◯
3. Water/ice mixed	—	—	—
4. Dry/wet ice mixed	—	—	—
5. Refrozen ice (wet)	✕	✕	◯
6. Snow covered (rough)	◯	◯	✕

er. Sun's angle of elevation was 26°). Characteristics of surface conditions based on visual observations are summarized in Table 3. Thin lake ice (~5 cm) with about 2 cm of snow cover showed low albedo in the near-infrared range. Snow with a rough surface showed also low albedo in near-infrared range. A rough surface consists of a combination of bright areas and shadow areas. A shadow area over snow has only the reflectance of diffused light, which has small intensity in the near-infrared range. There is strong spectral contrast between the intensities of visible and near-infrared in the shadow area of snow. A rough surface can have a small near-infrared/visible ratio. Since this study has only a few observation points, various surface types should be examined further. Based on the present results, the surface condition of sea ice observed by MESSR and AVNIR with low near-infrared albedo is considered to be a wet surface, ice particles suspended in sea water, or wet surface of thin ice.

5. Summary

There are problems in observing a thin ice area. A sea ice area of newly formed ice and sea ice area of low concentration have similar albedo in the visible range. Observation of sea ice using thermal brightness temperature is also difficult because the brightness temperature of thin sea ice is close to that of open water. From the result of analysis by visible and near-infrared radiometers aboard a satellite, it is confirmed that thin sea ice has a low N_{ir}/V_{is} ratio. Laboratory and field observations using visible and near-infrared spectrometers show that sea ice with a wet surface and suspended ice particles in water, show a great decrease of albedo in the near-infrared range compared to decrease of visible albedo. That reflects the small N_{ir}/V_{is} ratio.

This result is useful to detect frazil ice, and also to discriminate between low-concentrated ice cover and wet ice cover as the intensity of near-infrared decreases due to wet ice cover but not due to dry and sparse ice cover.

Acknowledgments

References

Enomoto, H. (1996): Observation of thin sea ice area in the Okhotsk Sea and impacts for climatological study. J. Remote Sensing Soc. Jpn., **16**, 100–111.

Enomoto, H., Warashina, H., Saito, T. and Shiraiwa, T. (1996): Interannual variability of sea ice conditions in Syowa Station sector deduced from DMSP SSM/I data. Proc. NIPR Symp. Polar Meteorol. Glaciol., **10**, 119–126.

NASDA EOC (1987): MOS-1 VTIR dêta CCT fômatto setsumeisho (Explanation of MOS-1 VTIR data

CCT format). Tokyo, Remote Sensing Technology Center of Japan.

ROGER, A. A., DAVID, G. B., KEVIN, M. and LEDREE, F. W. (1995): Spectral albedo of snow-covered first-year and multi-year sea ice during spring melt. Ann. Glaciol., **21**, 337–342.

USHIO, S. and WAKATSUCHI, M. (1993): A laboratory study on supercooling and frazil ice production processes in winter coastal polynyas. J. Geophys. Res., **98**, 20321–20328.

WEEKS, W. F. and ACKLEY, S. F. (1986): The growth, structure, and properties of sea ice. chapter 1. The Geophysics of Sea Ice, ed. by N. UNTERSTEINER. New York, Plenum Press, 9–164.